AFRL-AFOSR-VA-TR-2022-0048

Graphene microfluidics for dynamic, electron microscopic bio-imaging

Jiang, Xiaocheng
TRUSTEES OF TUFTS COLEGE INC
169 HOLLAND ST FL 3
SOMERVILLE, MA, 21442401
US

09/30/2021
Final Technical Report

Air Force Research Laboratory
Air Force Office of Scientific Research
Arlington, Virginia 22203
Air Force Materiel Command

REPORT DOCUMENTATION PAGE

Form Approved
OMB No. 0704-0188

1. REPORT DATE *(DD-MM-YYYY)*	**2. REPORT TYPE**	**3. DATES COVERED** *(From - To)*
30-09-2021	Final	15 Feb 2018 - 15 May 2021

4. TITLE AND SUBTITLE
Graphene microfluidics for dynamic, electron microscopic bio-imaging

5a. CONTRACT NUMBER

5b. GRANT NUMBER
FA9550-18-1-0128

5c. PROGRAM ELEMENT NUMBER
61102F

6. AUTHOR(S)
Xiaocheng Jiang

5d. PROJECT NUMBER

5e. TASK NUMBER

5f. WORK UNIT NUMBER

7. PERFORMING ORGANIZATION NAME(S) AND ADDRESS(ES)
TRUSTEES OF TUFTS COLEGE INC
169 HOLLAND ST FL 3
SOMERVILLE, MA 21442401
US

8. PERFORMING ORGANIZATION REPORT NUMBER

9. SPONSORING/MONITORING AGENCY NAME(S) AND ADDRESS(ES)
AF Office of Scientific Research
875 N. Randolph St. Room 3112
Arlington, VA 22203

10. SPONSOR/MONITOR'S ACRONYM(S)
AFRL/AFOSR RTB2

11. SPONSOR/MONITOR'S REPORT NUMBER(S)
AFRL-AFOSR-VA-TR-2022-0048

12. DISTRIBUTION/AVAILABILITY STATEMENT
A Distribution Unlimited: PB Public Release

13. SUPPLEMENTARY NOTES

14. ABSTRACT
We have developed graphene-based, electron-transparent interfaces to enable high-resolution structural and functional inquiry of fundamental biophysics using electron as the probe. In particular, we have been focusing on developing graphene microfluidic devices with two strategic approaches: (i) direct growth of graphene channels via chemical vapor deposition on microstructured metal catalysts; (ii) assembly of all-carbon based microfluidic device by transferring pregrown graphene onto patterned graphite substrate. Moreover, we have extended the scope of the research to use electron probes for functional biophysical inquiry.

15. SUBJECT TERMS

16. SECURITY CLASSIFICATION OF:			**17. LIMITATION OF ABSTRACT**	**18. NUMBER OF PAGES**	**19a. NAME OF RESPONSIBLE PERSON**
a. REPORT	**b. ABSTRACT**	**c. THIS PAGE**			SOFI BIN-SALAMON
U	U	U	UU	14	**19b. TELEPHONE NUMBER** *(Include area code)* 426-8411

Standard Form 298 (Rev.8/98)
Prescribed by ANSI Std. Z39.18

Final Performance Report

Grant Number: FA9550-18-1-0128

Project Title: Graphene microfluidics for dynamic, electron microscopic bio-imaging

Reporting Period: 02/15/2018 – 05/14/2021

Program Officer:

Dr. Sofi Bin-Salamon

Biophysics Program, AFOSR/RTB2

Email: sofi.bin-salamon@us.af.mil

Lead organization: Tufts University

Type of Business: Educational

PI: Xiaocheng Jiang

Department of Biomedical Engineering,
Tufts University, 4 Colby Street, Medford, MA 02155
xiaocheng.jiang@tufts.edu | O: (617) 627-0775 | F: (617) 627-3231

Admin POC: Dora Ramos

75 Kneeland Street, Boston, MA 02111

Dora.Ramos@tufts.edu | O: (617)627-8858

I. PROJECT OVERVIEW

This is the final report on the AFOSR program, "Graphene microfluidics for high-resolution, dynamic cell imaging with electron microscopy", carried out at the Tufts University, MA. The program was initiated in Feb. 15th 2018. The objective is to develop graphene-based, electron-transparent interfaces that will enable high-resolution structural and functional inquiry of fundamental biophysics using electron as the probe. As an imaging platform, the liquid impermeable, atomically thin, mechanically strong, and electrically transparent graphene channel could facilitate direct electron microscopic imaging of wet biological samples, and provide new insights about many biologically significant processes that are difficult to achieve with traditional optical or cryo electron microscopic methods.

During this project period, we have been focusing on developing graphene microfluidic devices with two strategic approaches: (i) direct growth of graphene channels via chemical vapor deposition (CVD) on microstructured metal catalysts; (ii) assembly of all-carbon based microfluidic device by transferring pre-grown graphene onto patterned graphite substrate. Moreover, we have extended the scope of the research to use electron probes for functional biophysical inquiry. Specifically, we developed a biosynthetic strategy to create graphene based, electron-transparent cellular interfaces *in-situ*. This carbon-based interface can mitigate the biotic-abiotic charge transport barrier by actively wiring the intercellular metabolic electron transfer chain to extracellular microelectrodes for further investigations and applications.

II. RESEARCH ACCOMPLISHMENTS

II.1. Bottom-up growth of graphene microfluidics on structured catalysts

Our efforts in this direction included the optimization of chemically synthesized graphene with different catalysis aiming at formation of large enough liquid impermeable graphene domains with limited number of carbon layers, which is a key factor for the transparency in electron microscopy. We have included our progress of developing a prototype graphene microfluidics using directly synthesized graphene microtubes. In addition, we have described our progress of developing substrate-based lithographically compatible fabrication of microfluidics with graphene imaging windows. Lastly, we have carried out proof-of-concept imaging studies under scanning electron microscope, which demonstrate the good electron transparency of graphene wall and its capability for preserving wet biological cells for high-resolution imaging.

II.1.A Development of prototype graphene microfluidic channels using chemically synthesized graphene microtubes.

We first try to test the fundamental concept and the properties of graphene microfluidics, using graphene microtubes via chemically synthesized on the surface of metal wires as a demonstration. As shown in Fig. 1, copper wire was brought to CVD to grow graphene on its surface. Then the copper wire with graphene coating was assembled onto substrate and sealed with high-vacuum

epoxy, leaving a certain distance of its length exposed as imaging domain. Last, the copper catalysis was chemically etched after the fabrication process.

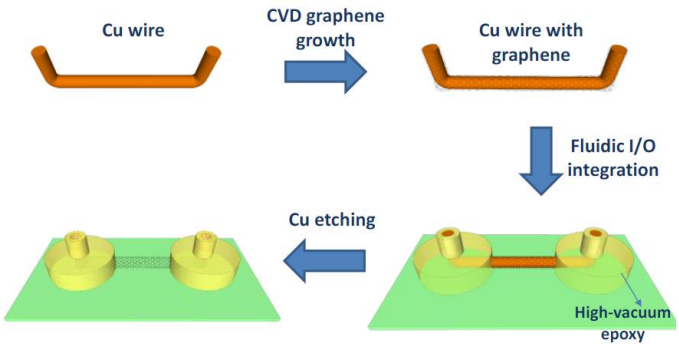

Fig. 1. Fabrication of prototype graphene microtubes

For example, 50 um diameter copper wires (Fig.2, A-C) were first electropolished to generate a smooth surface as required for high-quality graphene synthesis afterwards (Fig.2, D-F). The wire was then put into high vacuum CVD chamber for annealing followed by growth of graphene (Fig. 2, G-I). Duration, temperature, pressure and gas atmosphere were all tested for precisely control the properties of the grown graphene, such as domain size and thickness.

The graphene coated copper wires were firstly brought into copper etchant for liquid permeability test. Epoxy was used to cover the two ends of the wire and after curing, the whole sample was put into 2M $FeCl_3$ solution. Uniform etching of copper was observed along the length of the copper wire, suggesting that the graphene coating is not isolating the liquid from attacking interior copper.

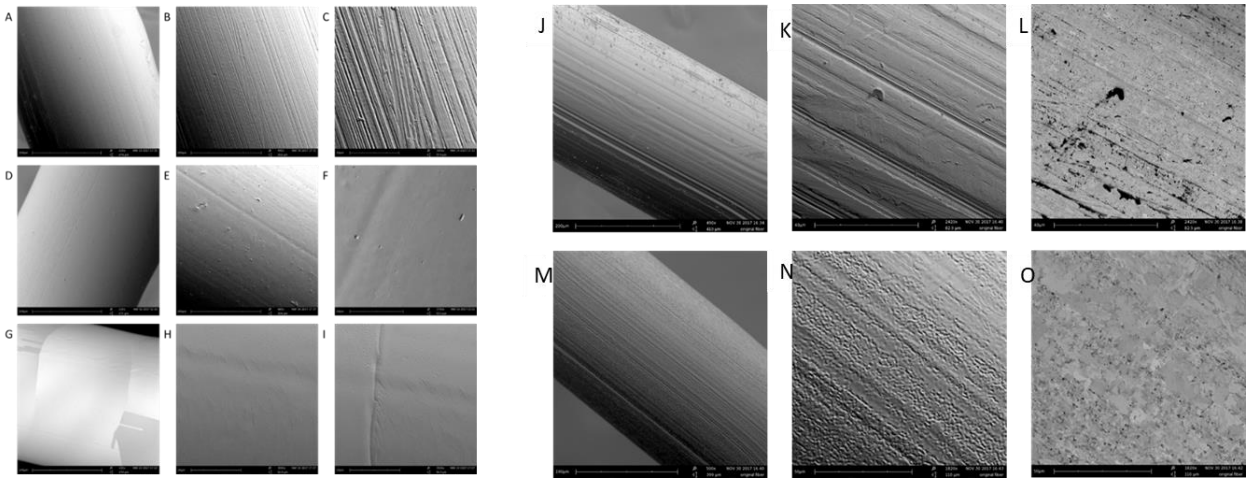

Fig. 2. Left: graphene synthesized on copper wires. (A-C) untreated copper wires; (D-F) electropolished copper wires; (G-I) graphene grown on copper wires. Right: graphene synthesized on nickel wires. (J-L) untreated nickel wires; (M-O) graphene grown on nickel wires.

To further tune the properties of grown graphene and improve the impermeability, we seek different metal catalysis for the CVD growth. We tested nickel wires (Fig. 2J-O) and copper/nickel alloy wires (Fig. 5) to this end. The copper/nickel alloy wires were prepared by first depositing nickel on the surface of copper wires while rotating the wires for uniform coating, and then annealed at high temperature (850-1000 ^{o}C) for varied length of time.

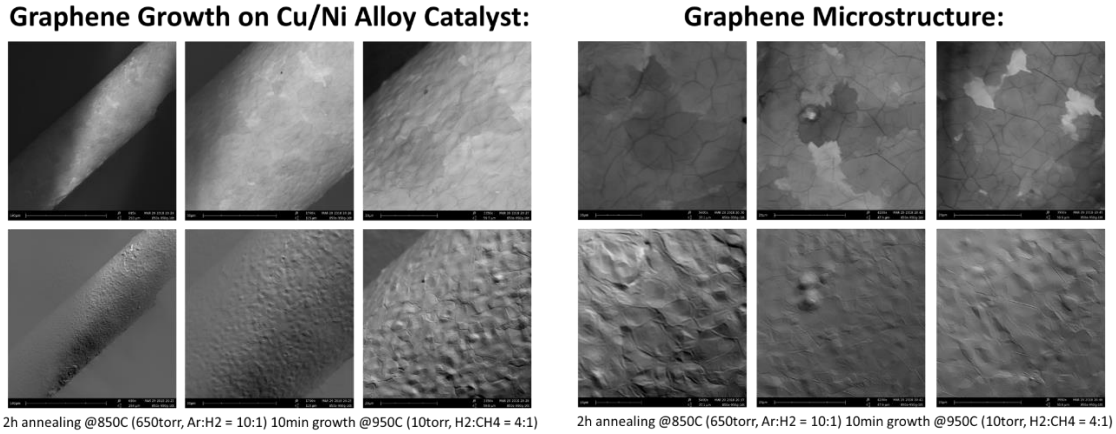

Fig. 3. Graphene synthesized on copper/nickel alloy wires.

These graphene growth samples with different catalysis and growth condition were later test for permeability in a similar way. They all showed length dependent leakage which is limited by the domain size/continuity size of the grown graphene, exceeding which leakage will happen. Among them, graphene grown on copper/nickel alloy wires didn't show any leakage when opening is below 100 um for 12 hours (Fig. 4), suggesting a suitable condition for robust graphene microtubes for liquid sealing and potentially for electron microscopy.

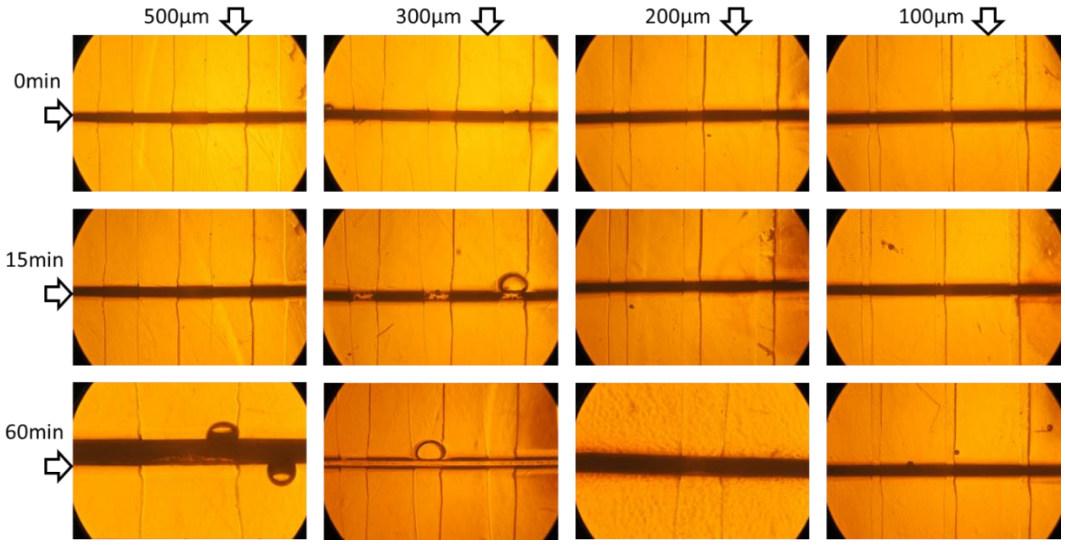

Fig. 4. Etching test of graphene synthesized on copper/nickel alloy wires. Top row: before etching; middle row: 15 min etching; bottom row: 60 min etching. Four columns indicate photoresist patterning with 500, 300, 200 and 100 um width openings.

As aforementioned, a prototype device with graphene microtubes has been demonstrated. Specifically, a thin layer of photoresist was spun coated; then wires with graphene were laid down on it and baked to fully embed the wires with graphene firmly on the substrate. Second, another layer of photo resist was spun coated on top of the construct with UV patterning to form windows for inset, outlet and imaging, while covering the other areas (Fig. 5, A-B). The imaging window was firstly covered by positive photoresist temporarily during the copper etching process through the two ends of the wires (Fig. 5, C-D). Last, the positive photoresist was removed by acetone.

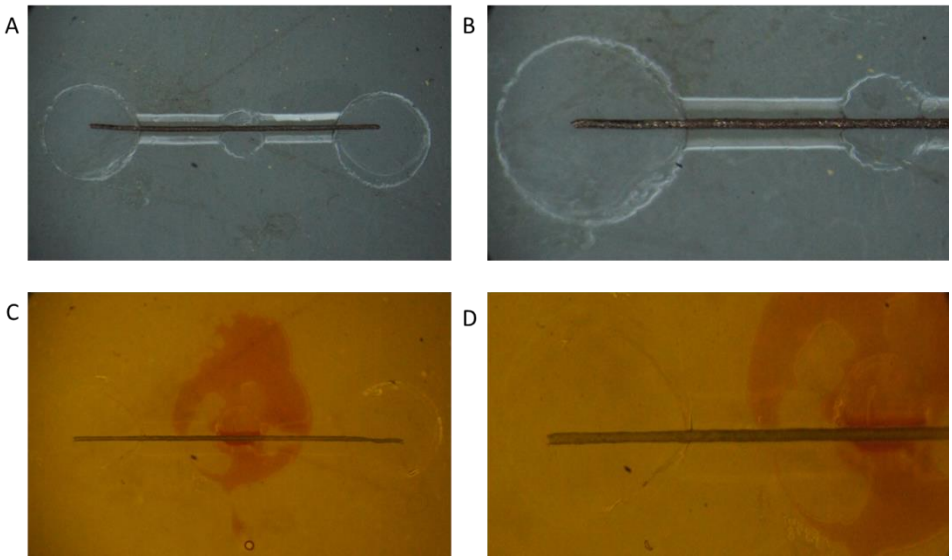

Fig. 5. Fabrication of graphene microtubes devices. (A-B) wire with graphene was embedded and pattern by SU-8 photoresist. Two bigger holes on each end is for the microfluidic inlet and outlet. The middle hole is for imaging. (C-D) The devices was then put into $FeCl_3$ etchant to etch the wire and form a continuous channel while the middle hole was protected temporarily by a drop of positive photoresist.

II.1.B On-chip graphene growth on patterned catalysts.

While the metal wire template represents a proof-of-the-concept for the graphene microfluidics, we seek to implement complete designable protocol for the fabrication. As shown in Fig. 6, the metal catalysis can be patterned by lithography for PCB compatible processes. We started out testing by using copper as the catalysis. Copper was first deposited onto silicon substrate followed by CVD synthesis. Similar problem of leakage occurs in this scenario because the graphene grown on the surface of pure copper doesn't protect the copper from being etched away, confirming the above results that graphene grown on copper surface is not continuous over a certain area. We also test and optimize the catalysts to tune the properties of as-grown graphene for improved continuity. Under optimal conditions, we have successfully demonstrated the fabrication of arrays of microfluidic devices on top of quartz substrate, using micropatterned Ni/Cu alloy as the catalysts (Fig. 7). Although the imaging window is still small (50 μm) and further optimization to increase the graphene domain size could broaden the capabilities of viewing different samples, the current results are encouraging as it fits the requirement for imaging cells or cell dynamics.

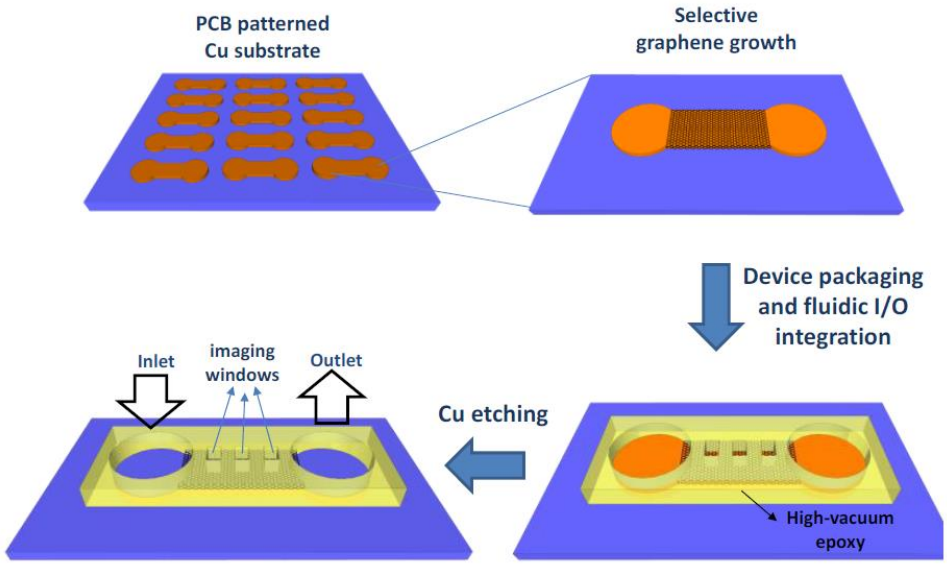

Fig. 6. Graphene microfluidics with PCB compatible processes.

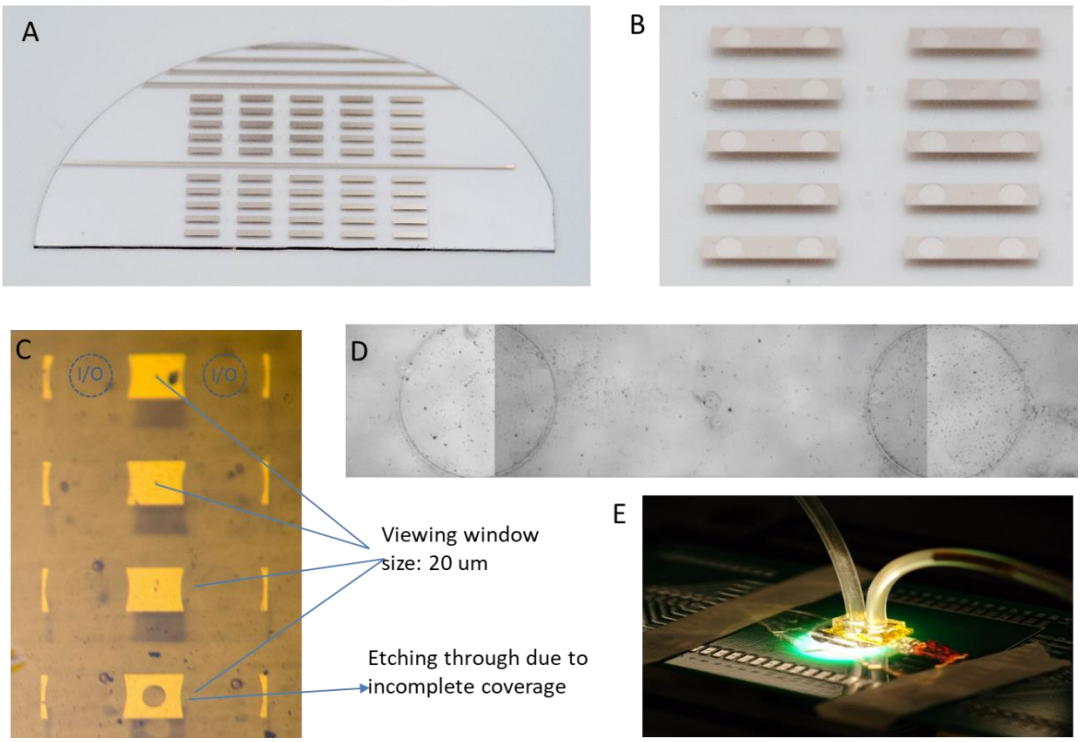

Fig. 7. (A) On-chip graphene growth on patterned Ni-Cu catalysts. (B) Defining of fluidic I/O and viewing windows using photolithography. (C) Metal catalyst removal and channel formation (in progress). (D) Bright-field image showing the on-chip graphene microfluidic channel after complete etaching. (E) Photograph of an assembled microfluidic device.

II.1.C Preliminary Imaging Test

We have further carried out imaging tests under scanning electron microscope to examine the potential of as-fabricated graphene microfluidic device for high-resolution imaging of wet specimen. Silver nanowires were first prepared and exploited as s model system, which yield similar contrast between samples with and without graphene coverage, demonstrating the high electron transparency of the graphene wall (Fig. 8A,B). Structural features as small as 10 nm can be clearly resolved under a low accelerating voltage of 3kV. Similarly, wet biological samples, such as *Shewanella loihica*, can be effectively encapsulated and imaged with minimal invasiveness under vacuum, preserving all the structural details (Fig. 8C), in contrast to the control sample which are completely dried without graphene sealing (Fig. 8D).

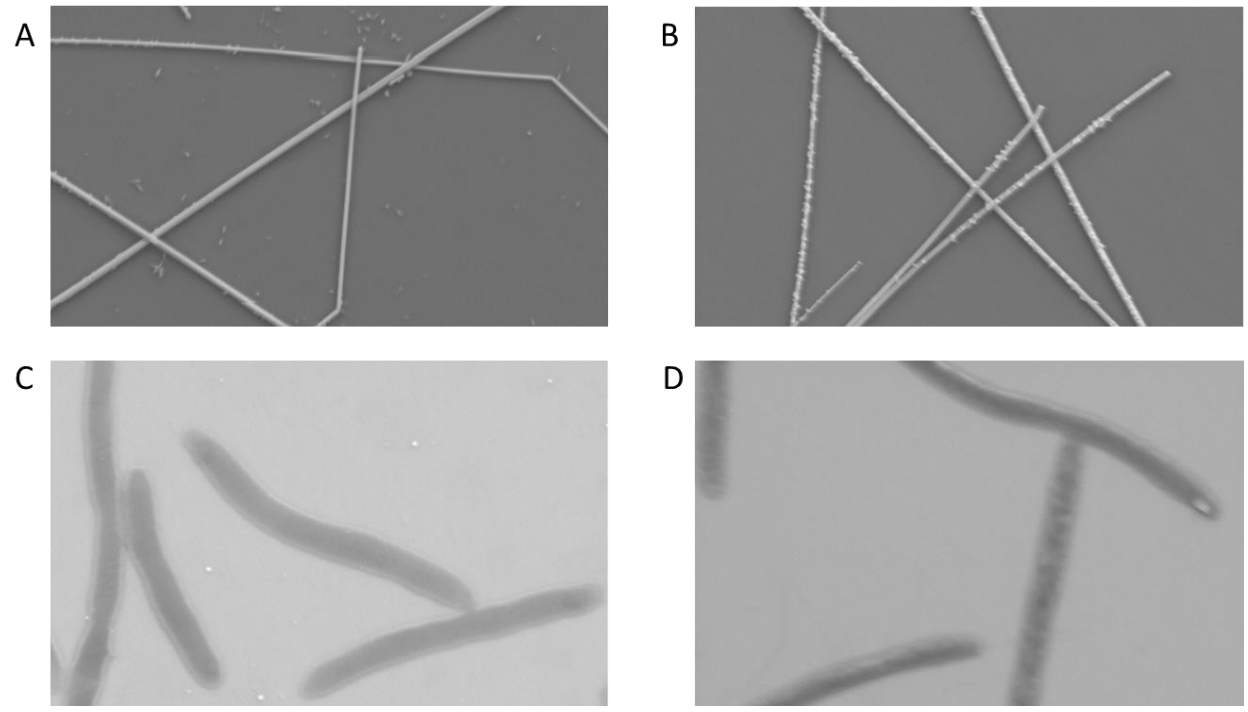

Fig. 8. Scanning electron microscopic imaging of silver nanowires (A,B) and *Shewanella loihica* with (left) and without (right) graphene coverage.

II.2. Development of an all-carbon based microfluidic imaging platform with transferred graphene

We further tested the idea of constructing graphene-based microfluidic devices through post-assembly of transferred graphene with patterned graphite substrate, where the strong π-π interaction is utilized to seal the device and achieve liquid impermeability.

II.2.A Micrometer Thick Graphite Substrates on silicon wafer through Peeling and Transfer

First, we optimize the peeling and transferring techniques to obtain a pure graphite sheet on silicon wafer, which can serve as the substrate for microfluidic device fabrications. The key

steps and parameters of these processes are summarized in Fig. 9. To start the process, a hundred micrometer thick graphite is peeled off from a highly oriented pyrolytic graphite (HOPG) crystals using Scotch tape. Before peeling, a uniform pressure is applied on the tape covered HOPG to strengthen the binding for obtaining peeled graphite layer with high surface smoothness as indicated by its mirror-like surface (Fig. 9, top right insert). Next, the Scotch tape supported graphite is transferred to the silicon wafer with 2 μm S1813 coated. Baking is then applied to solidify S1813 while promote the binding between graphite and S1813, simultaneously. In this study, the baking temperature is selected at 130 ˚C to ensure the permanent binding between graphite and silicon wafer, which can simplify the consecutive fabrication. After cooling to room temperature, the Scotch tape is detached from silicon wafer, where a graphite with around 10 μm thickness remain anchored and ready for microfabrication. The mirror-like surface implies the smooth surface of this transferred graphite.

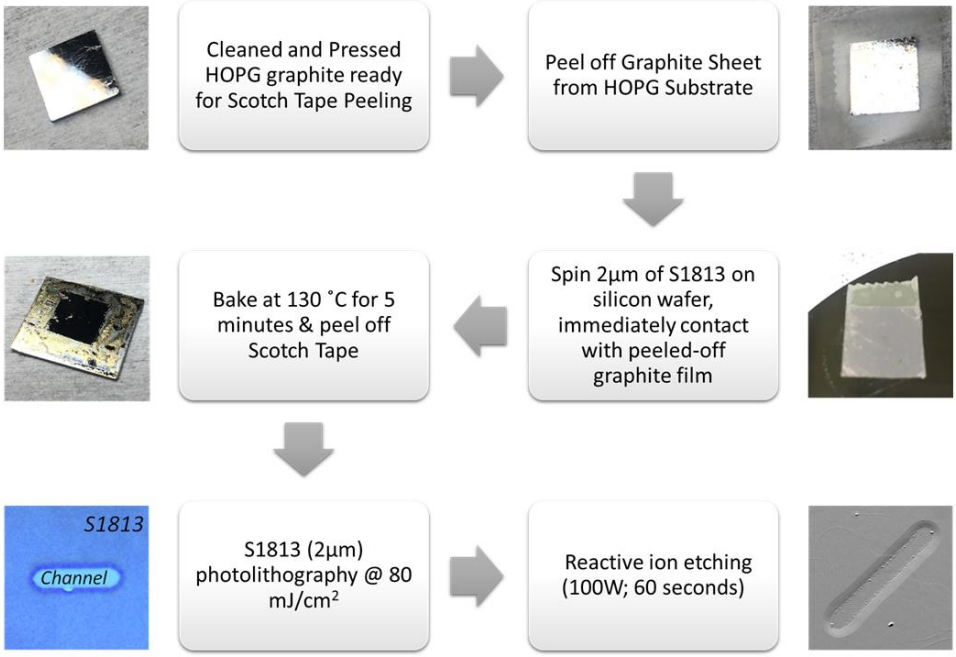

Fig. 9. Fabrication of graphite microchannels

II.2.B Microchannel Fabrication through Graphite lithography

Patterning the sacrificial photoresist layer for microchannel etching is based on the standard protocol of S1813 photolithography. In short, S1813 is spin-coated, UV exposed, and developed to obtain the projected microchannel opens on transferred graphite. The thickness and exposures of S1813 are optimized to facilitate the following fabrications. Specifically, 4 μm or thicker photoresist is required to avoid the depletion of sacrificial layer during etching. Besides, the exposure energy is selected at 80 mJ/cm^2 (for 4 μm), to obtained a under exposure S1813 which can compensate the undercut caused by the isotropic etching of graphite. Reactive ion etching (RIE) with 100W applied power under pure oxygen atmosphere is applied for microchannel fabrication. Typically, channel with 1.8 μm thickness can be obtained after a 60 second etching, which is

correlated to a 30 nm/second etching rate. Overall, this fabrication process possesses resolutions at 10 μm. The microstructures of fabricated microchannel is further investigated by SEM and the results is presented in Fig. 10. As shown in the images, this fabrication can obtain microchannels on a graphite substrate, of which, the nanoscale roughness may be attributed to the RIE process; whereas, damage is not observed on the graphite surrounding the microchannels as its surface remains smooth. It also has to emphasis that all the SEM images of microchannels are obtained without metal coating, which indicate that this process leads to with minimum-to-none contamination to the graphite substrate; hence the conductivity surface of graphite can be preserved. This smooth and conductive graphite substrate is desired for consecutive process in the imaging chamber construction though graphene transfer.

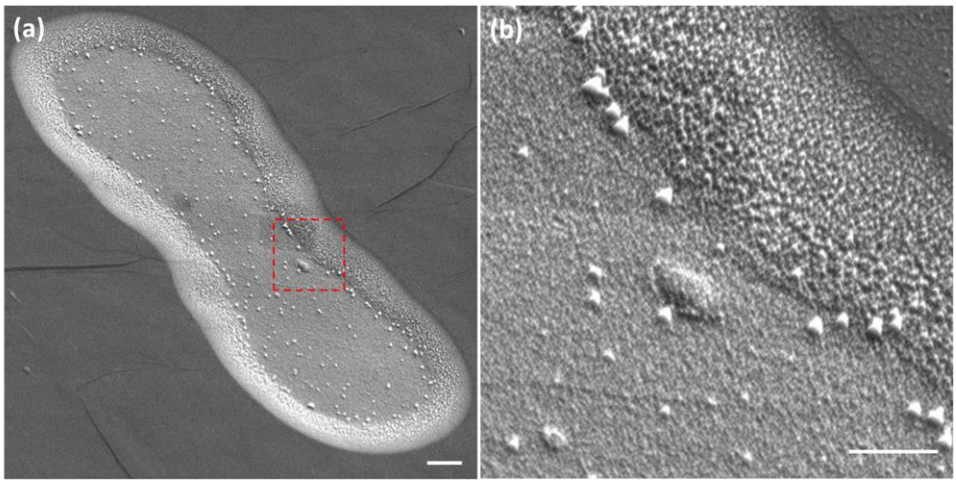

Fig. 10 SEM images of fabricated microfluidic channel on graphite substrate. (a) whole channel and (b) high magnification of the selected area indicated by the red dash-line in (a). In both images, the nanoscale roughness inside the microchannel is attributed to the RIE etching, while the un-etching area remain smooth.

II.2.C Implementation of Graphene Imaging Windows

After the microfabrications, a single layer graphene is exploited to seal the microchannels, which perform as both an air/liquid impermeable cover and an imaging window. Toward this aim, the chemical vapor deposition (CVD) is applied in graphene synthesis using a copper foil as the catalytic substrate. This CVD graphene is then covered on the microchannel using our customized procedures. First, the CVD graphene is coated with PMMA as intermediate materials for transfer. Following by the copper etching, washing and drying, the PMMA-coated graphene is transferred to a TEM grid that acts as a carrier that allow handling the graphene under a dry condition. After removing the PMMA, the graphene is brought into a close contact with graphite substrate, where the strong carbon-carbon interactions can occur and seal the microchannels. The SEM images show a conformal coverage of graphene layer on the graphite substrate, which also offers sufficient electron transparency as demonstrated by the visible nanoscale roughness on the surface of microchannels Fig. 11.

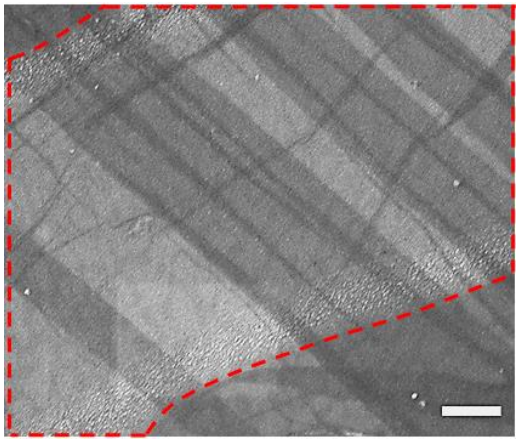

Fig. 11 SEM image of graphene covered microfluidic channel; the channel area is highlighted by the red dash-line.

II.2.D The *in-situ* SEM image inquiry of biomineralization process

Utilizing this all-carbon imaging chamber which offers superior sealing (under high vacuum environment) and electron transparency, we have demonstrated that the biomineralization process of *Shewanella loihica* can be observed *in-situ* under SEM with submicron resolution. As presented in both low-(Fig. 12A) and high- (Fig. 12B) magnification images, the gold nanoparticles (AuNPs) with size at 50-100 nm can be synthesized after introducing 10 mM hydrogen tetrachloroaurate into the culture solution of *Shewanella loihica* under anaerobic condition that known to promote the biomineralization.

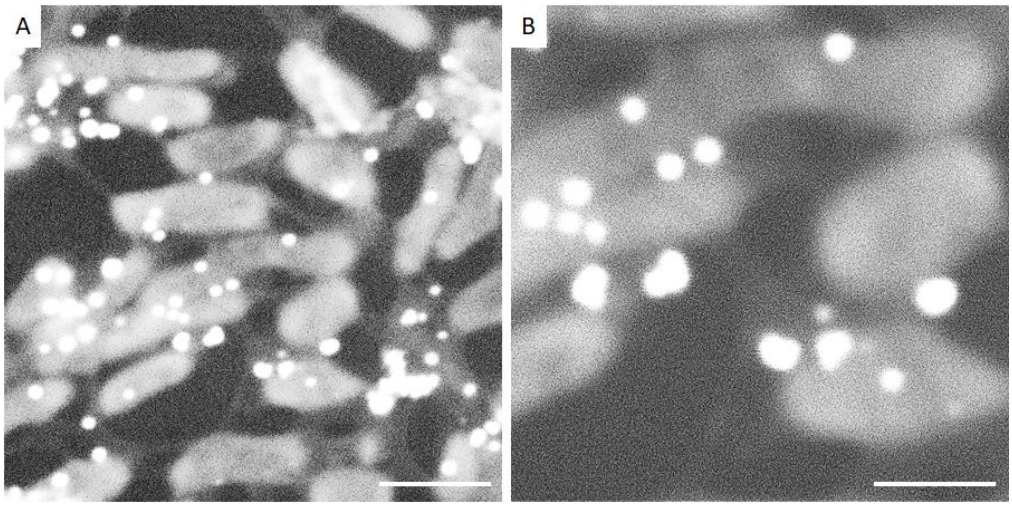

Fig. 12 The in-situ SEM image of gold nanoparticles (AuNPs) synthesized by the biomineralization of *Shewanella loihica* with (A) low- and (B) high- magnifications. Scale bar (A): 1 μm (B): 500 nm

Interestingly, most of bio-synthesized AuNPs are intimately connected with the outer membranes or membrane extensions of *Shewanella loihica*. This observation suggests that the extracellular electron transfer mediated by the conductive outer membrane proteins of *Shewanella loihica* can be the key biological function that underpin the biomineralization of AuNPs. In

addition, the clear observation of the protein-based membrane extensions further confirms the superior electron transparency of this device, which can be attributed to the graphene imaging window that can minimized the attenuation in electron signals (e.g. diffraction, reflection, absorption etc.) during imaging.

II.3 Electron-transparent interfaces for functional biophysical inquiry

We further extended the scope of the research to use electron probes for functional biophysical inquiry. Specifically, we developed a biosynthetic strategy to create graphene based, electron-transparent cellular interfaces in-situ. This carbon-based interface can mitigate the biotic-abiotic charge transport barrier by actively wiring the intercellular metabolic electron transfer chain to extracellular microelectrodes for further investigations and applications.

To synthesize the carbon-based bio-electronic interface, the extracellular electron transfers (EET) of *G. sulfurreducens* DL-1 (DL-1) is exploited to reduce GO into reduced graphene oxide (rGO) after contact with GO covered microelectrode. This graphene-based interface is utilized to study the electron transfer of *G. sulfurreducens*, which involves both ionic supported, redox driven electron transfers (ET), and tunneling-based intermolecular electron transports (ETp). To quantitatively investigate the interfacial ET, three-electrode cyclic voltammetry (CV) measurements are carried out. Voltammograms from both GO-covered and bare gold electrodes show redox activities attributable to the outer membrane cytochrome C (cytCs) of DL-1 biofilms (oxidation potential of around -0.3V and reduction potential of around -0.45 V v.s. Ag/AgCl). These results suggest that the introduction of rGO does not alter the mechanisms of redox-driven ETs in cytCs-based networks. However, the difference in CV profiles between gold/biofilm and rGO/biofilm indicated that the rGO can greatly improve the ET kinetics at the bio/electrode interfaces (Fig. 13(a)). In gold/biofilm, the low-current (± 0.36 μA), rate-limited (sigmoid-shaped) ET profiles in both positive (cytC oxidation, ET from biofilm to gold) and negative (cytC reduction,

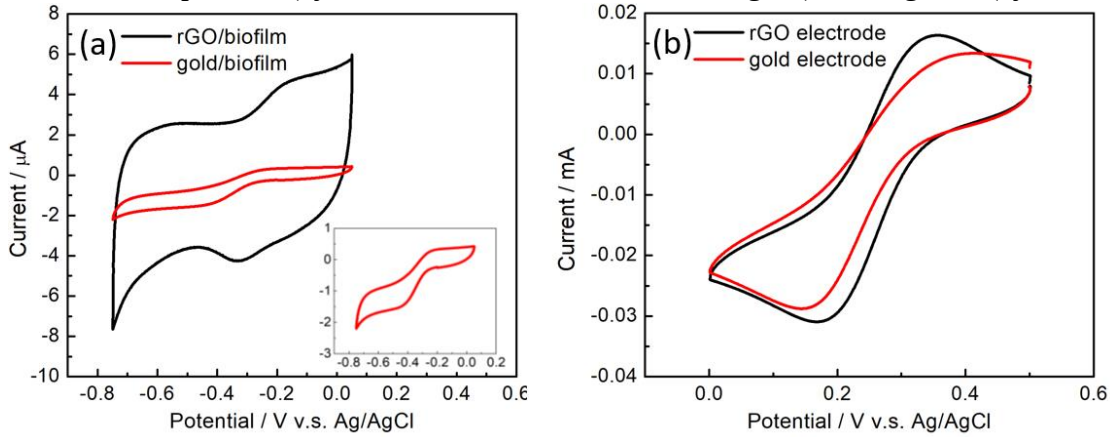

Fig. 13. Electrochemical characterizations of rGO/biofilm and gold/biofilm. (a) Cyclic voltammetry of rGO/biofilm and gold/biofilm. The black and red curves represent electron transfer currents at the rGO/biofilm and gold/biofilm interfaces, respectively. (electrolyte: bacteria culture media; applied potential: -0.8 to 0 V; scan rate: 10 mV/s). (b) Cyclic voltammetry of electrochemically active surface areas of both rGO covered, and pure gold electrodes (electrolyte: potassium ferricyanide (10 mM); applied potential: 0 to 0.5V scan rate: 10 mV/s).

ET from gold to biofilm) scans are led by the insufficient gold-cytC electrical coupling. In contrast, rGO/biofilm presented well-defined redox peaks of cytCs with enhanced current levels (± 5μA), consistent with faster, diffusion-limited ET process. To exclude the possibility that the larger current is associated with the increase of effective electrode area after GO coating/reduction, we have performed control CV tests on both electrodes in 10 mM ferricyanide after removing biofilms. Comparable current magnitudes were observed in the CV scans, indicating that the surface area change caused by GO coating is negligible (Fig. 13 (b)). Instead, we attribute the transformation in ET kinetics to the increased density of redox active cytCs as a result of more effective linkage through the biosynthesized rGO.

To fully decipher the ETp phenomenon in temporary domain, we have carried additional two-terminal measurements on dehydrated rGO/biofilm and gold/biofilm with either DC or AC inputs. For DC measurements, continuous potential sweeping is applied between ±1V with various scan rates to provide insight about charge transport under non-equilibrium conditions. For gold/biofilm, the source-drain current is minimal (< 0.5 nA) at low bias regime and shows exponential increase when the applied voltage is over ±0.4 V (red curve in Fig. 14 (a)). The tunneling barrier at small bias could be originating from non-optimal cytCs conformation/electrical contact, which could be overcome when the source-drain potential is raised above 0.4 V, bringing the HOMO-LUMO of cytCs and golds into resonance. In comparison, the measurement from rGO/biofilm sample shows much larger current without noticeable evidence for contact barrier within the measured voltage range (black curve in Fig. 14 (a)). Instead, substantial hysteresis, indicative of charge trapping, has been recorded during voltage sweeping, and becomes more significant with the increase of scanning rate. We believe this capacitive effect is associated with the detained electron transport across the biofilm as a result of additional electrostatic energy barriers when supporting electrolytes/counter ions are removed (thus reduced charge screening).

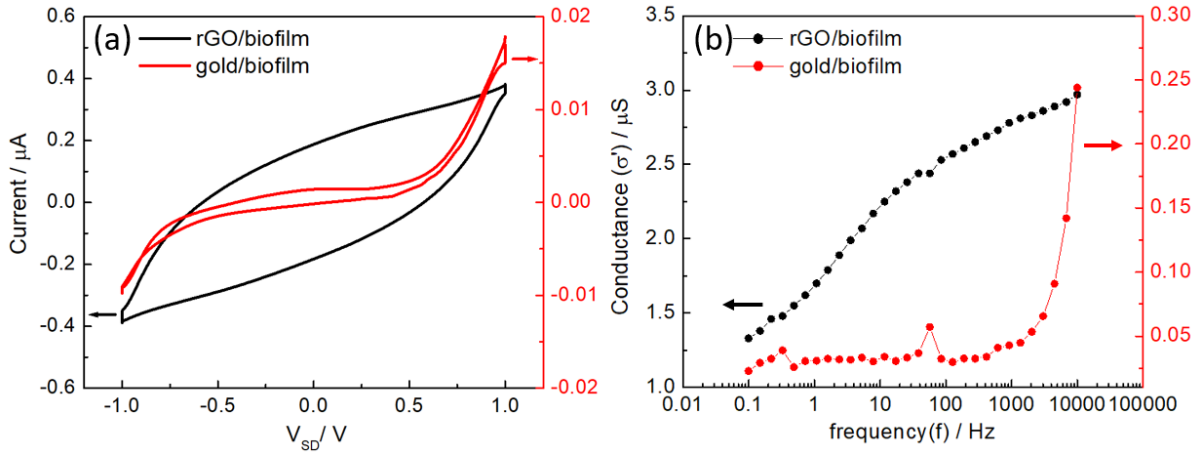

Fig. 14. Cross biofilm electron transport measurements of rGO/biofilm and gold/biofilm of (a) DC inputs, the black and red curves represent the source-drain currents of rGO/biofilm and gold/biofilm, respectively (sweep between ±1 V, scan rate: 80 mV/s); (b) AC inputs, the black and red curves represent frequency-dependent impedances of rGO/biofilm and gold/biofilm, respectively. (applied bias: 0V, frequency: 0.1-10^4 (Hz)).

This behavior could be obscured by the non-optimal contact/slow ETp rate across the contact barrier, and only becomes prominent when the interfacial electron transport is no longer a limiting factor. These results further demonstrate the potential of our strategy to interrogate the intrinsic ETp properties of electroactive biofilms as well as other biological charge transport systems. The two-terminal AC measurements are also conducted to investigate their frequency dependent response. For the bare gold contact, the AC conductance of the *G. sulfurreducens* biofilm is composed of a low-frequency plateau and a dispersive high-frequency region with the critical frequency at 1000 Hz (red curve in Fig. 14 (b)), which can be modeled as a parallel resistance and capacity circuit. At low frequency, ETp is restricted by the interfacial energy barrier as discussed in the DC measurement. When applying frequency above critical point, the electrical field induce extra energy to overcome the barrier that contribute to the dramatic increase of AC conductance. Overall, these AC conductance measurements suggested that the ETp across our *G. sulfurreducens* biofilms is a hopping-driven process. While without rGO, charge transfer is dominated by the gold-biofilm interface which limits the ETp efficiency of the whole system. In summary, taking advantage of the active bio-reduction of GO, we demonstrated the possibility to seamless merge the microbial and inorganic electron transports. These biosynthetic materials interface significantly enhanced both the ion-supported ET and the solid state ETp processes at the gold-biofilm interface, which has been hindering the unambiguous understanding of the charge transfer mechanisms in biosystems and biotic-abiotic interfaces as well as the potential applications in bioelectronics.

Moving forward, we further exploit this bio-synthetic strategy to realize synergic bioelectronic interface with another biological charge transport system. In particular, the photosynthetic redox center (Cyt b6f protein) on Anabaena, a type of cyanobacteria, is actively "wired" toward external electrodes using bio-reduced GO, which allows the full access of the photosynthetic electron transfer chain of Anabaena. As demonstrate in the results (Fig. 15 (a)), the redox of Cyt b6f protein can be precisely detected (0.2 V and -0.2 V, respectively) with rGO interface; whereas, these redox peaks cannot be observed when directly contact Anabaena with electrodes (Fig. 15 (a) insert). This observation indicates the critical role of rGO in wiring the photosynthetic electron transfer chain with external electrodes. This discover is further advocated the significant increase in photo-responsive current (80 nA) on the electrode with rGO interface as compared with bare bio-electrode contact (40 nA) (Fig. 15 (b)). Overall, this research suggests that the bio-reduced graphene oxide can be a universal strategy to create a electron transparent functional interface to seamlessly wire biological components with synthetic electronics for ultimately promoting the quality of our biophysical research.

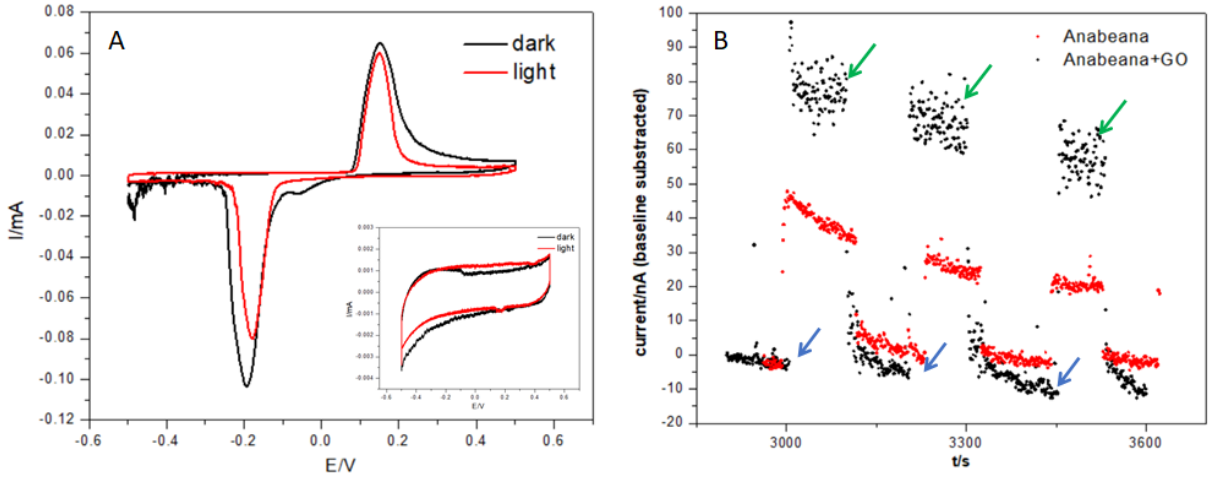

Fig. 15. Measurements of photosynthetic electron transfer chain of Anabaena (a) electrochemical characterizations of the redox center (Cyt b6f protein) on Anabaena under light (red) and dark (black) condition with rGO interface. (insert: same measurements without rGO interface); (b) electrical measurement of photosynthetic electron transfer chain of Anabaena with and without rGO interface, of which, the blue and green arrows indicate the on and off of simulated sun light, respectively.